(10.4), (01.8), (01.2), and (00.1) Twin Laws of Calcite ($CaCO_3$): Equilibrium Geometry of the Twin Boundary Interfaces and Twinning Energy

ARTICLE *in* CRYSTAL GROWTH & DESIGN · JULY 2010

Impact Factor: 4.89 · DOI: 10.1021/cg100233p

5 AUTHORS, INCLUDING:

Marco Bruno
Università degli Studi di Torino
84 PUBLICATIONS **706** CITATIONS
SEE PROFILE

Marco Rubbo
Università degli Studi di Torino
98 PUBLICATIONS **614** CITATIONS
SEE PROFILE

Mauro Prencipe
Università degli Studi di Torino
74 PUBLICATIONS **1,127** CITATIONS
SEE PROFILE

Dino Aquilano
Università degli Studi di Torino
190 PUBLICATIONS **1,000** CITATIONS
SEE PROFILE

DOI: 10.1021/cg100233p

CRYSTAL GROWTH & DESIGN Article

2010, Vol. 10
3102–3109

(10.4), (01.8), (01.2), and (00.1) Twin Laws of Calcite ($CaCO_3$): Equilibrium Geometry of the Twin Boundary Interfaces and Twinning Energy

Marco Bruno,* Francesco Roberto Massaro, Marco Rubbo, Mauro Prencipe, and Dino Aquilano

Dipartimento di Scienze Mineralogiche e Petrologiche, Università degli Studi di Torino, Via Valperga Caluso 35, I-10125 Torino, Italy

Received February 18, 2010; Revised Manuscript Received May 4, 2010

ABSTRACT: The "Four Twin Laws of Calcite", expressed by their twin planes (10.4, 01.8, 01.2 and 0.01, hexagonal frame) have been investigated in order to assess the structure of the interfaces between twinned individuals. Athermal twinning and adhesion energies were evaluated by calculations using empirical potential functions: the relaxed interfaces were modeled to minimize the surface energy. To this end, different configurations of the twin interfaces have been considered when surface reconstructions were needed to cancel out the surface dipole moment, which is intrinsic to the ideal interfaces of both the (00.1) and (01.2) twins. Calculation shows that (*i*) the (00.1) twin law is the most likely to occur, and (*ii*) the minimum of the twinning energy is obtained if the twin operation is a diad axis perpendicular to the (00.1) interface. Finally, it has been demonstrated that the (00.1) twins are the only ones that can be generated by a 2D heterogeneous nucleation mechanism, while the 3D (either homogeneous or heterogeneous) nucleation is the dominating mechanism for the other twins.

1. Introduction

Twinning in calcite ($CaCO_3$, space group $R\bar{3}c$, hexagonal frame) has been known for about 150 years; it is commonly accepted that there are only four different kinds of twins in calcite ("The Four Twin Laws of Calcite"[1]), which describe all possible twins produced either by deformation or during crystal growth (Figure 1). These laws are expressed by the twin planes (TP) $c = \{00.1\}$, $r = \{10.4\}$, $e = \{01.8\}$, and $f = \{01.2\}$ which coincide with the original composition planes (OCP). In particular, the main deformation twinning planes of calcite are $\{01.8\}$ and $\{10.4\}$,[2−4] although deformation twinning has also been reported on the $\{01.2\}$ planes.[5] Only recently, Pokroy et al.,[6] by using X-ray diffraction, found a formerly unknown twin form in calcite crystals artificially grown from a solution to which a mollusc shell-derived 17-kDa protein (Caspartin) was added. This newly observed twin form is characterized by the (10.8) twin plane. Nevertheless, since we are interested in studying naturally grown twinned calcite crystals, in the following we deal with the "Four Twin Laws of Calcite", only.

It is worth noting that, at variance with the $\{10.4\}$ and $\{01.8\}$ forms, the ideal surfaces of both the $\{01.2\}$ and $\{00.1\}$ forms exhibit iso-oriented dipoles in their external layers (type-3 surfaces, according to the Tasker's classification[7]), since they are made of alternating lattice planes populated by either Ca^{2+} or CO_3^{2-} ions. Thus, the ideal $\{01.2\}$ and $\{00.1\}$ forms are electrically unstable. The mechanisms required to stabilize such dipolar surfaces can be (i) surface modifications at the atomic level induced by adsorption of foreign substances; (ii) reconstruction of the surfaces to cancel out the dipole moment, and/or (iii) rearrangement of the electronic structure, resulting in an effective charge transfer between the polar surfaces, as was suggested for some forms of covalent phases.[8,9]

*Corresponding author. E-mail: marco.bruno@unito.it. Telephone: +390116705131. Fax: +390116705128.

The $\{01.2\}$ form was stabilized by considering two surface reconstructions and two alternative terminations (either Ca or CO_3 ions).[10] The dipole moment was deleted by removing 50% of the ion rows in the outermost layer, in two different ways:

(i) in the first mode (R1 reconstruction henceforth), the direction of the removed rows was chosen arbitrarily, i.e. without constraints imposed by the bulk symmetry;
(ii) in the second one (R2 reconstruction), the removed rows respected the glide planes perpendicular to $\{01.2\}$ faces, according to the bulk crystal symmetry.

The $\{00.1\}$ form was stabilized by considering two surface reconstructions as well:[11]

(i) The R1 reconstruction was carried out by modifying the outermost layer only. As in the previous case, half of the $\langle 100 \rangle$ rows (either Ca ions or CO_3 groups) were removed from the outermost plane of the $\{00.1\}$ slab, without respecting the bulk symmetry.
(ii) The R2 reconstruction, named "octopolar reconstruction",[12] was achieved by removing 75% of the ions in the outer layer and 25% of the other ionic species in the layer beneath it, thus preserving the 3-fold symmetry of the $\{00.1\}$ form.

The labels R1 and R2 were used for both the $\{01.2\}$ and $\{00.1\}$ forms, to distinguish between a surface reconstruction respectively breaking (R1) or preserving (R2) the bulk crystal symmetry. Therefore, to distinguish among the different surface reconstructions and terminations of the $\{01.2\}$ and $\{00.1\}$ forms, we will use here the notation $(hk.l)_A^B$, where A = R1 or R2 and B = Ca or CO_3.

Starting from these considerations and by adopting a two-dimensional slab model, in this work we aimed at the determination of the equilibrium geometry at 0 K of the (10.4), (01.8), (01.2), and (00.1) twin boundary interfaces. Since the experimental techniques cannot provide a detailed description of the structural modifications induced by a

 Published on Web 06/03/2010

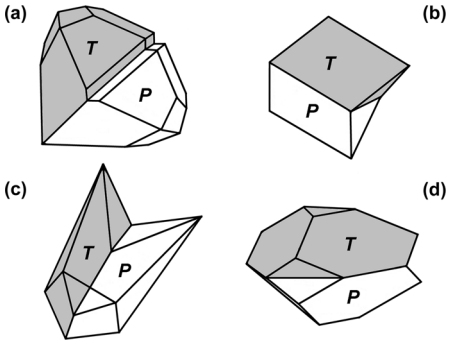

Figure 1. The four twin laws of calcite: (a) (10.4); (b) (01.8); (c) (01.2); (d) (00.1). Twinned crystals redrawn from ref 23.

planar defect such as a twin boundary, such information can only be achieved through geometry optimizations performed by means of empirical or quantum mechanical calculations. We decided on empirical calculations since, due to the complexity of our system, the quantum-mechanical approach would be too demanding; on the other hand, a reliable empirical potential[13] is available, which reproduces, very satisfactorily, both the bulk and the surface structures of calcite.

The twinning energy (the work required to form a unit area of the twin interface) and the adhesion energy (the energy, per unit area, recovered when the two separated individuals are composed to form the twin) were also calculated. Twinning energy is a key thermodynamical quantity for the determination of the equilibrium morphology of twins and the estimation of their most probable mechanism of formation during growth. We also report some considerations on the probability to obtain twins during growth in aqueous solution through 2D or 3D nucleation.

The structure of the paper is as follows: (1) description of the computational parameters and the strategy used in the geometry optimizations of the twinned slabs; (2) presentation of the results, together with their interpretation.

2. Computational Details

Calculations (optimization of the slab geometries and twinning energies) were performed by using the interatomic potential function for calcite developed by Rohl et al.[13] and the General Lattice Utility Program (GULP) simulation code.[14] Rohl et al.[13] obtained the potential parameters by fitting structural data for both calcite and aragonite, as well as physical properties (elastic and dielectric constants) and phonon frequencies. We used this empirical potential because it reproduces very successfully (i) the equilibrium geometry of the bulk crystal,[13] (ii) the equilibrium geometries and the surface energy values of the {01.2} and {10.4} faces obtained from *ab initio* calculations at the DFT (density functional theory; B3LYP Hamiltonian[15]) level,[10,11] as well as (iii) the experimental observations of the surface relaxation of the {10.4} form.[13] Geometry optimization is considered converged when the gradient tolerance and the function tolerance (*gtol* and *ftol* adimensional parameters in GULP) are smaller than 10^{-4} and 10^{-5}, respectively.

2.1. Slab Geometry Optimization. To investigate the (10.4), (01.8), (01.2), and (00.1) twin boundaries, a 2D-slab model was adopted.[16] A twinned slab, made by slabs 1 and 2 (Figure 2), was generated in the following way:

(i) slab 1 of a given thickness was made by cutting the bulk structure parallel to the *hk.l* twin plane of interest (10.4, 01.8, 01.2, and 00.1);

(ii) slab 2 was made by applying the appropriate twin law to the atomic coordinates of slab 1.

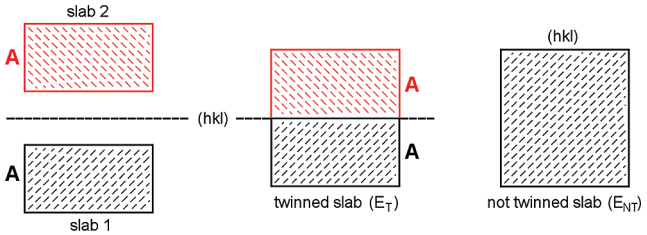

Figure 2. Scheme of a (*hkl*) twinned slab and of the not twinned slab.

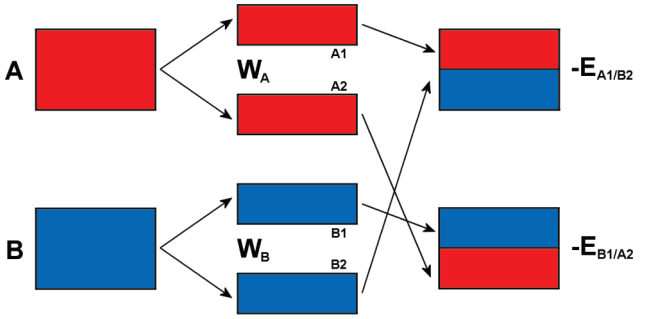

Figure 3. Schematized procedure to generate the A1/B2 and B1/A2 interfaces, starting from the A and B blocks.

Then, the twinned slab geometry (atomic coordinates) was optimized by considering all the atoms free to move, with the optimization being performed by means of the Newton−Raphson method. The calculation was done by considering the (10.4), (01.8), (01.2), and (00.1) twinned slabs with thickness up to 28, 60, 24, and 26 layers, respectively, which are sufficient to obtain an accurate description of the twinned interfaces. The slab thickness is considered appropriate when the relaxation of the outermost layers of the twinned slab does not affect the equilibrium geometry of the twin boundary interface or, in other words, when the bulklike properties are reproduced at the center of slabs 1 and 2 (Figure 2).

Tables listing lattice parameters and atomic coordinates of the optimized twinned slabs are available on request.

Preliminarily, and in order to obtain electrically neutral and nonpolar slabs, the (01.2) and (00.1) slabs were reconstructed (R1 and R2) by eliminating the atoms in excess. For both the (01.2) and (00.1) faces, this was obtained by using a (2 × 2) unit cell, whose axis lengths (*a* and *b*) were doubled with respect to the original ones.

The calculation on the (10.4) and (10.8) faces was instead performed by considering a (1 × 1) cell.

It is worth stressing that the type of surface reconstruction does not affect the relaxation of the twin boundary interface only if the thickness of the twinned slab satisfies the condition previously described.

2.2. Twinning and Adhesion Energies. The twinning energy, γ_{TE} (J/m^2), is the excess energy required to form a unit area of the twin boundary interface and reads

$$\gamma_{TE} = \frac{E_T - E_{NT}}{S} \quad (1)$$

where E_T and E_{NT} are the energies of the optimized twinned and not twinned slabs (Figure 2), respectively, and S is the area of the surface unit cell. As for the equilibrium geometry, when the thickness of the slab satisfies the convergence criterion, the γ_{TE} value is independent of the type of surface reconstruction.

As we know the twinning energy γ_{TE} (eq 1), we can calculate the adhesion energy of twinning, using the Dupré's relation[17] and the relevant surface energies. Section 2.3 is devoted to the surface energies, while, in the following, we reformulate the Dupré's relation to tackle the polar surfaces facing some of the twin interfaces studied in this work.

Let us consider two blocks, A and B (Figure 3), and let us separate them along the area S, thus doing the work $W_A + W_B$. Further, we suppose that all the surfaces so generated (A1, A2, B1, and B2) are different (e.g., different termination). Then, the half blocks are

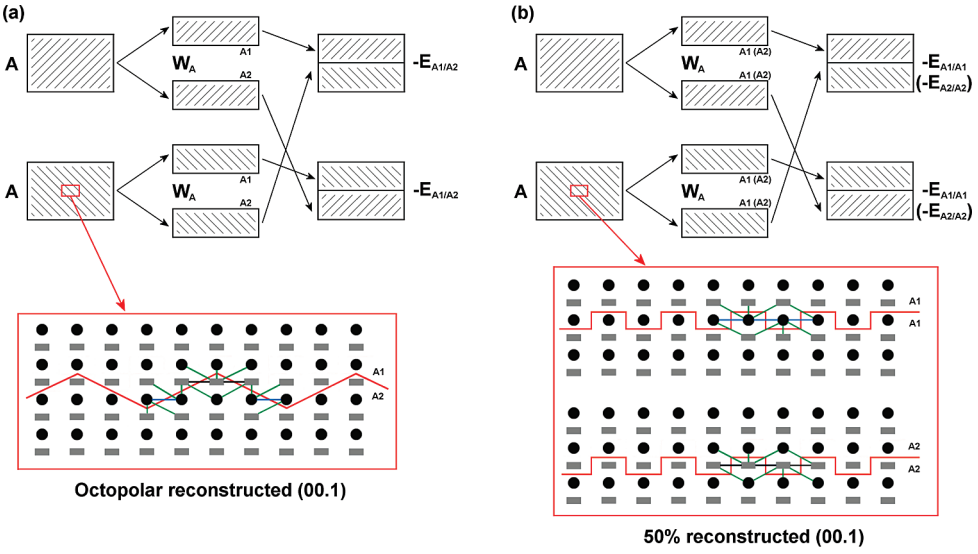

Figure 4. Generating a twinned slab having (a) A1/A2 and (b) A1/A1 or A2/A2 interfaces.

permuted and joined, thus recovering the adhesion energy $-(E_{A1/B2} + E_{B1/A2})$. The excess energy $(W_{A1/B2} + W_{B1/A2})$ resulting from the generation of the two interfaces A1/B2 and B1/A2 is

$$W_{A1/B2} + W_{B1/A2} = W_A + W_B - E_{A1/B2} - E_{B1/A2} \quad (2)$$

The total separation work $(W_A + W_B)$ can also be expressed as the algebraic sum of the works needed to generate the unrelaxed surfaces (W^u) and the relaxation energies (W^r):

$$W_A + W_B = (W^u_{A1} + W^r_{A1} + W^u_{A2} + W^r_{A2}) + (W^u_{B1} + W^r_{B1} + W^u_{B2} + W^r_{B2}) \quad (3)$$

where W^u_{A1}, W^u_{A2}, W^u_{B1} , and W^u_{B2} are the energies supplied to the system to create the unrelaxed surfaces A1, A2, B1, and B2, respectively, whereas W^r_{A1}, W^r_{A2}, W^r_{B1}, and W^r_{B2} are the corresponding relaxation energies. Putting eq 3 into eq 2, the following results:

$$W_{A1/B2} + W_{B1/A2} = (W^u_{A1} + W^u_{A2}) + (W^r_{A1} + W^r_{A2}) + (W^u_{B1} + W^u_{B2}) + (W^r_{B1} + W^r_{B2}) - (E_{A1/B2} + E_{B1/A2}) \quad (4)$$

Dividing by $2S$ both members of eq 4, one obtains

$$\langle\gamma_{AB}\rangle = \langle\gamma^u_A\rangle + \langle\Delta\gamma^r_A\rangle + \langle\gamma^u_B\rangle + \langle\Delta\gamma^r_B\rangle - \langle\beta_{AB}\rangle \quad (5)$$

where (i) the excess $\langle\gamma_{AB}\rangle = (W_{A1/B2} + W_{B1/A2})/2S$ is the averaged interfacial energy; (ii) $\langle\gamma^u_A\rangle = (W^u_{A1} + W^u_{A2})/2S$ and $\langle\gamma^u_B\rangle = (W^u_{B1} + W^u_{B2})/2S$ are the averaged unrelaxed surface energies of the A and B faces, respectively; (iii) $\langle\Delta\gamma^r_A\rangle = (W^r_{A1} + W^r_{A2})/2S$ and $\langle\Delta\gamma^r_B\rangle = (W^r_{B1} + W^r_{B2})/2S$ are the averaged work per unit area needed to relax the A and B faces; and (iv) $-\langle\beta_{AB}\rangle = -(E_{A1/B2} + E_{B1/A2})/2S$ is the average specific adhesion energy, representing the energy gained by joining A1 to B2 and B1 to A2. Now, since the average relaxed surface energies of the A and B faces can also be written as $\langle\gamma^r_A\rangle = \langle\gamma^u_A\rangle + \langle\Delta\gamma^r_A\rangle$ and $\langle\gamma^r_B\rangle = \langle\gamma^u_B\rangle + \langle\Delta\gamma^r_B\rangle$, eq 5 simplifies to

$$\langle\gamma_{AB}\rangle = \langle\gamma^r_A\rangle + \langle\gamma^r_B\rangle - \langle\beta_{AB}\rangle \quad (6)$$

This is nothing but the generalized Dupré's relation (as for the case drawn in Figure 3), which reduces to the classical Dupré's relation, $\gamma_{AB} = \gamma^r_A + \gamma^r_B - \beta_{AB}$, when A1 = A2 = A and B1 = B2 = B.

Let us now write the Dupré's relation for the (00.1) twin of calcite. As the 00.1 twin plane coupled with the inversion center of the crystal is equivalent to a diad symmetry axis normal to the twin plane, the two blocks of calcite (A) are related by a 2-fold axis (Figure 4). By cutting block A, we can generate two different surface configurations, according to the type of surface reconstruction:

(i) Two complementary octopolar faces (R2 reconstruction), A1 = $(00.1)^{Ca}_{R2}$ and A2 = $(00.1)^{CO_3}_{R2}$ (Figure 4a), which have equal unrelaxed surfaces energies, $\gamma^u_{(00.1)^{Ca}_{R2}} = \gamma^u_{(00.1)^{CO_3}_{R2}}$, but different relaxed surface energies, $\gamma^r_{(00.1)^{Ca}_{R2}} \neq \gamma^r_{(00.1)^{CO_3}_{R2}}$.[11]

(ii) Two identical R1 reconstructed faces, A1 = $(00.1)^{Ca}_{R1}$ or A2 = $(00.1)^{CO_3}_{R1}$ (Figure 4b). In this case, both the unrelaxed and the relaxed surface energies are different, $\gamma^u_{(00.1)^{Ca}_{R1}} \neq \gamma^u_{(00.1)^{CO_3}_{R1}}$ and $\gamma^r_{(00.1)^{Ca}_{R1}} \neq \gamma^r_{(00.1)^{CO_3}_{R1}}$.[11]

It is not surprising that the unrelaxed surface energies of the octopolar reconstructed faces are equal. This can be justified by considering that, at variance with the R1 reconstruction, the separation work needed to generate the two terminations (Ca or CO_3) of the octopolar reconstructed face must be the same. This is evident when observing the schematic representation of the R1 and R2 reconstructions (Figure 4): in particular, by only considering the first nearest neighbors, one has to break eight Ca−CO_3 *bonds* and three Ca−Ca interactions in order to generate the A1 ≡ $(00.1)^{Ca}_{R1}$ face, whereas eight Ca−CO_3 and three CO_3−CO_3 interactions should be interrupted to generate the A2 ≡ $(00.1)^{CO_3}_{R1}$ face (Figure 4b). Then, the different values of the unrelaxed surface energies of the $(00.1)^{Ca}_{R1}$ and $(00.1)^{CO_3}_{R1}$ faces are due to the differences between the Ca−Ca and CO_3−CO_3 interactions. Instead, two Ca−Ca, two CO_3−CO_3, and twelve Ca-CO_3 couples have to be broken to generate both the A1 ≡ $(00.1)^{Ca}_{R2}$ and A2 ≡ $(00.1)^{CO_3}_{R2}$ faces (Figure 4a). This implies equivalence of the $(00.1)^{Ca}_{R2}$ and $(00.1)^{CO_3}_{R2}$ unrelaxed surface energies.

When considering the octopolar reconstruction (Figure 4a), the relation $W^u_{A1} = W^u_{A2} = W^u_A$ is valid; eq 4 then becomes

$$W_{A1/A2} = 2W^u_A + (W^r_{A1} + W^r_{A2}) - E_{A1/A2} \quad (7)$$

and the Dupré's relation reads

$$\gamma_{TE} = \gamma_{AA} = 2\langle\gamma^r_A\rangle - \beta_{AA} \quad (8)$$

Instead, from the R1 reconstruction (Figure 4b), one obtains

$$W_{A1/A1} = 2W^u_{A1} + 2W^r_{A1} - E_{A1/A1} \quad (9)$$

or

$$W_{A2/A2} = 2W^u_{A2} + 2W^r_{A2} - E_{A2/A2} \quad (10)$$

and the Dupré's relation transforms into

$$\gamma_{TE} = \gamma_{AA} = 2\gamma^r_A - \beta_{AA} \quad (11)$$

where $\gamma^r_A = (W^u_{A1} + W^r_{A1})/S$ and $\beta_{AA} = E_{A1/A1}/S$ when two A1 surfaces are generated by the crystal cut, whereas $\gamma^r_A = (W^u_{A2} + W^r_{A2})/S$ and $\beta_{AA} = E_{A2/A2}/S$ when two A2 surfaces are created.

It is worth stressing that the γ_{TE} value does not depend on the type of interface between the twinned individuals; that is, eqs 8 and 11 must yield the same value of the (00.1) twinning energy, as is clear from eq 1, where γ_{TE} is not a function of the interface configuration. Equation 11 also applies to the (01.2) twinned slab, which allows two 50% reconstructions.

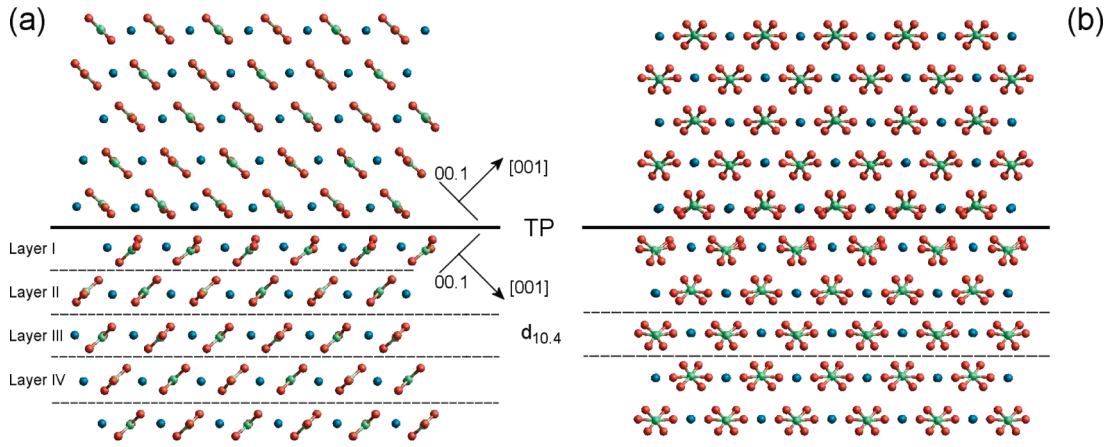

Figure 5. Relaxed structure of the (10.4) twin boundary interface. The (10.4) twinned slab is viewed along the ⟨010⟩ (a) and ⟨42$\bar{1}$⟩ (b) directions.

Putting eq 1 in eqs 8 and 11, one obtains:

$$\beta_{AA} = 2\langle\gamma_A^r\rangle - \gamma_{TE} = 2\langle\gamma_A^r\rangle - \frac{E_T - E_{NT}}{S} \quad (12)$$

$$\beta_{AA} = 2\gamma_A^r - \gamma_{TE} = 2\gamma_A^r - \frac{E_T - E_{NT}}{S} \quad (13)$$

Equation 12 only applies to the octopolar reconstruction of the (00.1) face, whereas eq 13 is valid for any 50% reconstruction. Depending on the range of the adhesion energy (β_{AA}), γ_{TE} assumes the following values:

(i)
$$\beta_{AA} = 0 \rightarrow \gamma_{TE} = 2\langle\gamma_A^r\rangle \text{ or } \gamma_{TE} = 2\gamma_A^r$$

(ii)
$$0 < \beta_{AA} < 2\langle\gamma_A^r\rangle \text{ or } 0 < \beta_{AA} < 2\gamma_A^r \rightarrow 0 < \gamma_{TE} < 2\langle\gamma_A^r\rangle \text{ or } 0 < \gamma_{TE} < 2\gamma_A^r$$

(iii)
$$\beta_{AA} = 2\langle\gamma_A^r\rangle \text{ or } \beta_{AA} = 2\gamma_A^r \rightarrow \gamma_{TE} = 0$$

Twinning is not allowed when the limiting condition (i) is fulfilled, while the opposite extreme condition (iii) implies that the specific work required to separate the two portions of the twin is equal to the one required to separate a not twinned crystal along the same plane. For the intermediate cases (ii), the probability to obtain a twinned crystal increases with the adhesion energy β_{AA}.

2.3. Calculation of the Surface Energy. The surface energies at 0 K of the relaxed (optimized) (10.4), (01.2), and (00.1) faces were determined in previous works[10,11,13] by using the Rohl et al.[13] potential, whereas the optimized structure and the surface energy of the (01.8) face (both unrelaxed and relaxed) have been determined in this work. The geometry optimization was done by considering the (01.8) slab subdivided into two regions: region 1, containing the surface and the underlying atomic layers that are allowed to relax, and region 2 which contains the same number of layers of region 1 and where no relaxation is assumed to occur. According to the standard two-region strategy employed by GULP, the surface energy is evaluated from the energy of the surface block of the crystal (region 1, U_s) and the energy of a portion of bulk crystal (U_b) containing the same number of atoms as the surface block:[18]

$$\gamma = \frac{U_s - U_b}{S} \quad (14)$$

A slab composed of eight layers in both regions 1 and 2 is sufficient to reach convergence on the γ values.

3. Results and Discussion

3.1. The (10.4) Twin Boundary Interface. The equilibrium geometry of the (10.4) twin boundary interface obtained with the force field method is reported in Figure 5. According to the (10.4) twin law, the two parts of the twin are related by a mirror parallel to the 10.4 plane. In this plane, the minimum surface unit cells of the two individuals making up the twinned slab are reciprocally translated by $^1/_{12}\langle\bar{4}41\rangle$ = 3.21 Å (Figure 6a); the unit cells are defined by the $^1/_3\langle42\bar{1}\rangle$ and ⟨010⟩ vectors, and their area is 40.34 Å^2.

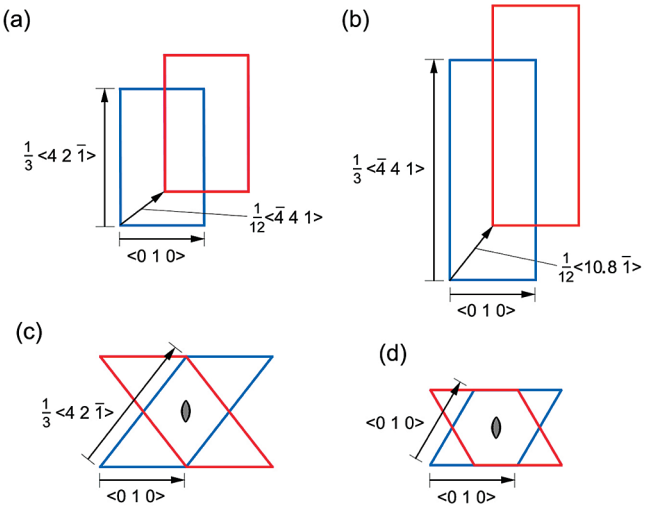

Figure 6. Surface 2D unit cells and origins of the (a) (10.4), (b) (01.8), (c) (01.2), and (d) (00.1) twinned slabs. Different colors indicate parent and twinned parts of the slab.

At the twin boundary interface, a structural relaxation sets in and propagates symmetrically toward the two portions of the twin. This mainly involves five $d_{10.4}$ layers in each portion. In particular, a large modification of the thickness of these slices is observed: as a matter of fact, $d_{10.4}$ results to be 3.24, 2.81, 3.17, 2.91, and 3.12 Å for layers I−V, respectively, whereas, in the bulk, the equidistance is 3.03 Å. Furthermore, the (10.4) layer at the twin boundary interface (layer I) shows a higher distortion with respect to either layers II−IV or the ideal bulk geometry: in particular, the CO_3 groups are rotated about the [001] axis and slightly tilted in the 00.1 plane. Due to this relaxation, a strong variation of the Ca−O distances is observed on going from the first layer (layer I in Figure 7a; i.e. the (10.4) layer at the twin interface) to the underlying ones (2.3813−2.6873 Å; Figure 7a). On the contrary, no significant variations of the C−O distances have been observed through the twinned slab, so that the CO_3 group seems to behave like a rigid unit (Figure 7a).

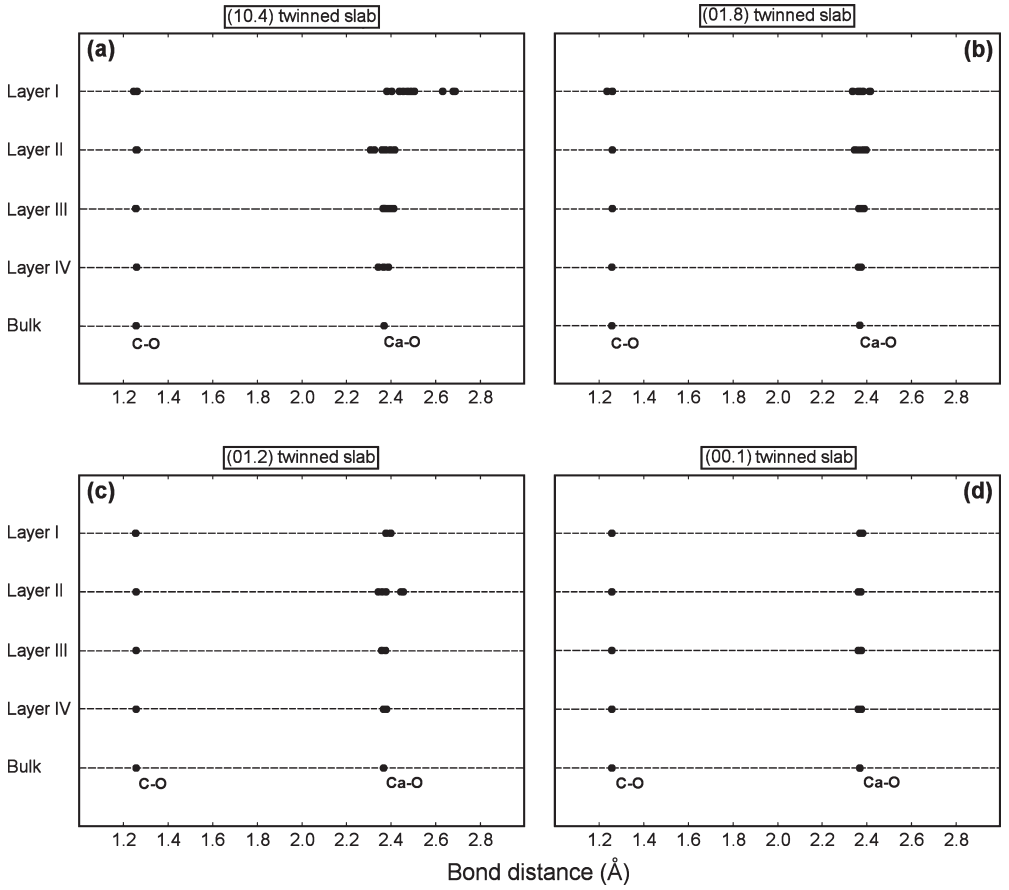

Figure 7. C−O and Ca−O distances as a function of layer depth in the (a) (10.4), (b) (01.8), (c) (01.2), and (d) (00.1) twinned slabs. The C−O and Ca−O distances in the bulk are also quoted for comparison.

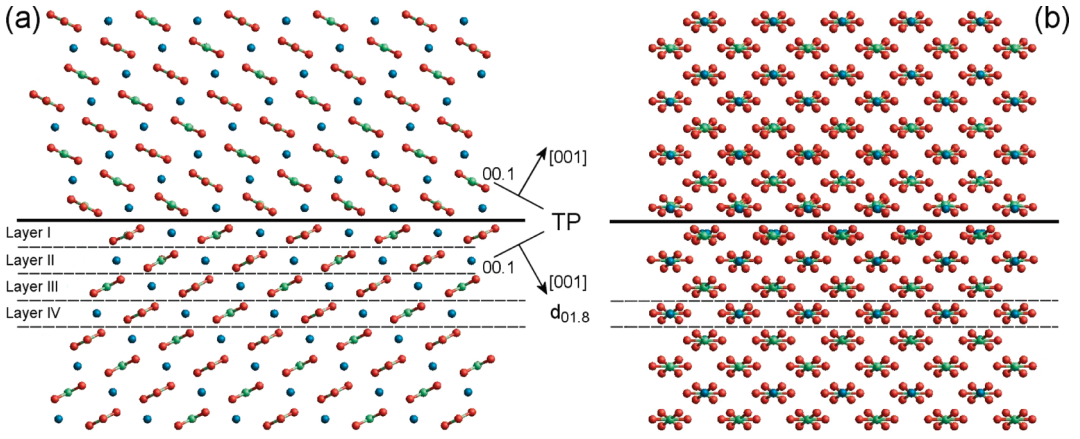

Figure 8. Relaxed structure of the (01.8) twin boundary interface. The (01.8) twinned slab is viewed along the (a) ⟨010⟩ and (b) ⟨$\bar{4}$41⟩ directions.

3.2. The (01.8) Twin Boundary Interface. The equilibrium geometry of the (01.8) twin boundary interface is drawn in Figure 8. According to this twin law, the two parts of the twinned crystal are related by a mirror parallel to the 01.8 plane. The minimum surface unit cells of the two individuals making up the twinned slab are translated by a segment $^{1}/_{12}\langle 10.8\bar{1}\rangle$ = 4.07 Å; their unit cells are defined by the $^{1}/_{3}\langle\bar{4}41\rangle$ and ⟨010⟩ vectors, and their area is 63.89 Å^2.

As for the (10.4) twinned slab, the (01.8) twin interface produces a relaxation of the structure, which involves mainly five $d_{01.8}$ layers in each portion of the twinned crystal. Their thickness, in proximity of the boundary interface, is significantly different with respect to that in the crystal bulk. As a matter of fact, $d_{01.8}$ is 2.01, 1.83, 1.98, 1.85, and 1.96 Å for layers I−V, respectively, whereas $d_{01.8}$ = 1.89 Å in the bulk. At variance with the (10.4) twinned slab, only the CO_3 groups in layer I are slightly tilted in the 00.1 plane, and only the Ca−O distances in layers I and II (2.3339−2.4160 Å; Figure 7b) do significantly vary with respect to that in the bulk (2.3685 Å).

3.3. The (01.2) Twin Boundary Interface. The equilibrium geometry of the (01.2) twin boundary interface is illustrated in Figure 9. According to the (01.2) twin law, the two parts of the twinned crystal are related by a 2-fold axis perpendicular

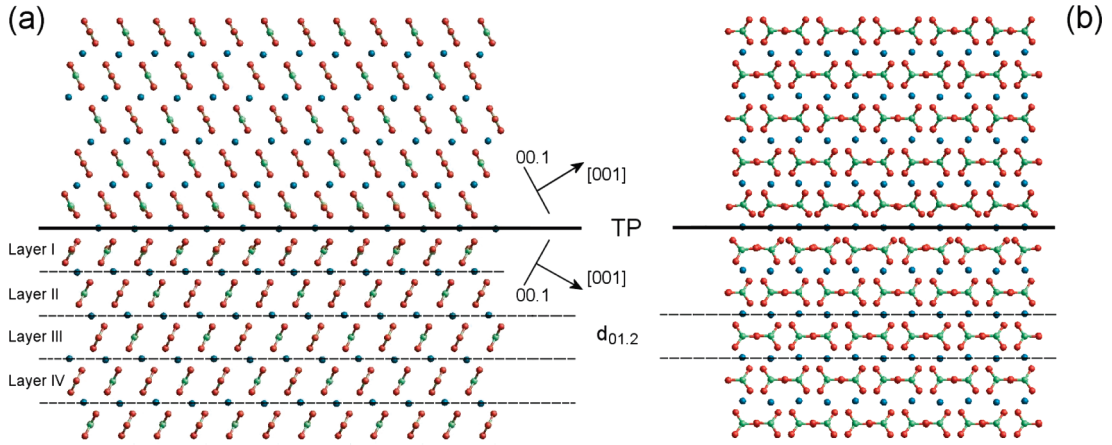

Figure 9. Relaxed structure of the (01.2) twin boundary interface. The (01.2) twinned slab is viewed along the (a) ⟨010⟩ and (b) ⟨12$\bar{1}$⟩ directions.

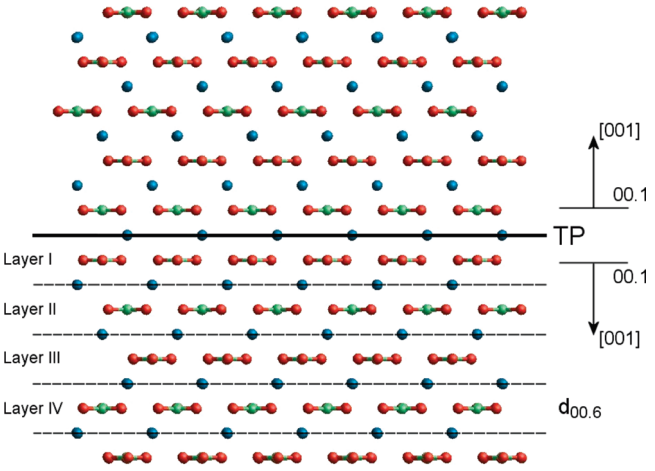

Figure 10. Relaxed structure of the (00.1) twin boundary interface. The (00.1) twinned slab is viewed along the ⟨010⟩ direction.

Table 1. Twinning Energies Calculated by Using eq 1

	(10.4)	(01.8)	(01.2)	(00.1)
γ_{TE} (J/m^2)	0.162	0.183	0.259	0.001

Table 2. Unrelaxed (γ^u) and Relaxed (γ^r) Surface Energies of the (10.4), (01.8), (01.2), and (00.1) Faces[a]

face	γ^u (J/m^2)	γ^r (J/m^2)	β_{AA} (J/m^2)
(10.4)	0.707	0.534	0.906
(01.8)	1.252	0.702	1.221
$(01.2)^{Ca}_{R1}$	3.402	0.953	1.647
$(01.2)^{CO_3}_{R1}$	3.791	0.982	1.705
$(01.2)^{Ca}_{R2}$	2.719	1.040	1.821
$(01.2)^{CO_3}_{R2}$	3.661	0.750	1.241
$(00.1)^{Ca}_{R1}$	2.476	0.834	1.667
$(00.1)^{CO_3}_{R1}$	1.720	0.764	1.527
$(00.1)^{Ca}_{R2}$	1.654	0.849	1.559
$(00.1)^{CO_3}_{R2}$	1.654	0.711	

[a] Specific adhesion energies (β_{AA}) are related to the (10.4), (01.8), (01.2), and (00.1) twin laws.

to the 01.2 plane (Figure 6c). As in the case of the (10.4) twinned slab, the unit cells are defined by the $^1/_3$ ⟨42$\bar{1}$⟩ and ⟨010⟩ vectors, with their area being 34.93 Å^2. At variance with the previous cases, a very slight relaxation is observed at the (01.2) boundary interface. In fact, the thicknesses of layers I−V (3.82, 3.85, 3.86, 3.86, and 3.85 Å, respectively) are very close to the $d_{01.2}$ value of the bulk (3.85 Å). Furthermore, only in layer I are the CO_3 groups slightly tilted in the 00.1 plane and rotated about the [001] axis, and only in layer II do the Ca−O distances differ significantly from that in the bulk (Figure 7c).

3.4. The (00.1) Twin Boundary Interface. Figure 10 shows the equilibrium geometry of the (00.1) twin interface. According to the (00.1) twin law, the two parts of the twin are related by a 2-fold axis perpendicular to the 00.1 plane (Figure 6d). The unit cells are defined by two equivalent ⟨010⟩ vectors, and their area is 21.48 Å^2. The 00.1 planar defect introduced by the twinning does not produce significant changes in the two portions of the twinned slab. Indeed, no rotations of the CO_3 groups and no variations of the Ca−O and C−O distances have been observed through the twinned slab (Figure 7d). Only the $d_{00.6}$ thickness of the layer I (2.86 Å) is slightly different with respect to the corresponding value in the bulk (2.84 Å).

3.5. Twinning Energies. The twinning and adhesion energies related to the (10.4), (01.8), (01.2), and (00.1) twin laws at 0 K are quoted in Tables 1 and 2, respectively. Owing to the very small difference between the energies of a twinned and nontwinned crystal, a very low value of $\gamma_{TE} = 0.001$ J/m^2 for the (00.1) twin law was determined. This is the excess energy required to generate a twinned (00.1) interface formed by two calcite individuals facing through the (00.1) interface and related by a 2-fold axis coinciding with the [001] axis (Figure 10; labeled C1 configuration hereinafter). The C1 configuration is energetically favored with respect to that where the two facing layers of CO_3 stack along the [001] direction but preserve the same orientation (labeled C2 configuration hereinafter) as if the twin operation was a 00.1 mirror plane; in this case the twinning energy would be $\gamma_{TE} = 0.084$ J/m^2, an order of magnitude greater than that of the C1 configuration. The equilibrium geometry of the twinned slab having the C2 configuration is not discussed; tables listing the lattice parameters and atomic coordinates of the optimized twinned slab are available upon request.

3.6. Mechanism of Formation of Calcite Twinned Crystals. The calculation of the twinning energies, γ_{TE}, has been addressed as a particular case of epitaxy by Stranski and Kaishew in a series of articles.[19] Subsequently, their works were developed by Kern[20] and Simon[21] in order to ground on thermodynamics the classification of twins by Friedel[22] and to unravel the mechanism of formation of twinned crystals: (i) formation of 2D or 3D nuclei, in twinned position, on a

Table 3. Area Occupied by a $CaCO_3$ Growth Unit, a_m, on the (10.4), (01.8), (01.2), and (00.1) Surfaces and the Minimum Value of the Calcite Supersaturation (Q_0) Required To Obtain a Twinned Crystal

	(10.4)	(01.8)	(01.2)	(00.1)
a_m (m^2)	20.17×10^{-20}	31.94×10^{-20}	17.46×10^{-20}	21.48×10^{-20}
Q_0	2.81×10^3	1.48×10^6	5.93×10^4	1.05

face of a pre-existing crystal (2D or 3D heterogeneous nucleation), or (ii) formation of a 3D twinned nucleus (3D homogeneous nucleation). In the following we apply to contact twins of calcite the conclusions reached by these researchers.

At high supersaturation, the activation energy for the formation of a twinned calcite bicrystal by three-dimensional homogeneous nucleation is always higher and the frequency of nucleation of twins is lower than that for the nucleation of a single crystal, as it is $\gamma_{TE} > 0$ in all the studied twin laws.

At relatively lower supersaturation, three-dimensional nucleation of normal or twinned embryos (critical nuclei) can occur on the crystal faces. The activation energy (ΔG_{3D}) of this process depends on the difference $\gamma_{TE} - \gamma^\circ$, with γ° being the surface energy of the face of the parent crystal supporting the embryo (eq 20, p 64, in ref 21):

$$\Delta G_{3D} = \frac{4[\sum_i c_i\gamma_i + (\gamma_{TE} - \gamma^\circ)c^\circ]^3}{27(\Delta\mu)^2} \quad (15)$$

where c_i and c° are shape factors, γ_i is the surface energy of the i-th free face of the 3D embryo, and $\Delta\mu$ is the thermodynamical supersaturation. As $\gamma_{TE} = 0$ corresponds to an embryo in normal position, the more twins occur by this mechanism, the lower the value of the twinning energy. Thus, excluding the (00.1) face, which deserves further consideration, this mechanism of twinning is more frequent on the (10.4) faces.

The very low value of γ_{TE} for the C1 configuration is strictly related to the high adhesion energies (Table 2), whose values are nearly equal to twice the surface energies, $\beta_{AA} \approx 2\langle\gamma^r_{(00.1)}\rangle$ (or $\beta_{AA} \approx 2\gamma^r_{(00.1)}$, according to the kind of surface reconstruction considered). This suggests a high probability of occurrence of stacking faults ($d_{00.6}$ layers with C1 configuration) along the [001] growth direction. Furthermore, in such a circumstance, the nucleation of a two-dimensional embryo in a twin position can occur. If one wants to make finite the number of units making the embryo and positive the activation barrier, ΔG_{2D}, the denominator of

$$\Delta G_{2D} = \frac{(\sum_l c_l\rho_l)^2}{4[\Delta\mu - a_m\gamma_{TE}]} \quad (16)$$

must be positive. In eq 16, ρ_l and c_l are the free edge energy and the shape factor of the l-th edge of the 2D embryo, respectively, while a_m is the area occupied by a $CaCO_3$ growth unit on the face considered (Table 3). To give an estimate and for the sake of a comparison of the twins studied, let us consider an aqueous solution where $\Delta\mu = kT \ln Q$, k is Boltzmann's constant, T is the absolute temperature, and $Q = (a_{Ca^{2+}}a_{CO_3^{2-}})/K_{sp,calcite}$ is the ratio between the effective ionic activity product and the calcite solubility product ($K_{sp,calcite}$), in the aqueous solution. Since $\Delta G_{2D} > 0$, the minimum value of the calcite supersaturation, Q_0, needed to obtain a twinned crystal is $Q_0 = \exp(a_m\gamma_{TE}/kT)$.

The Q_0 values for the different twin laws were calculated (Table 3) at $T = 298$ K using the twinning energies previously determined (Table 1). Extremely high values of Q_0 ($> 10^3$) were obtained for the (10.4), (01.8), and (01.2) twin laws, whereas a slight supersaturation ($Q_0 = 1.05$) is sufficient to nucleate a 2D embryo on the (00.1) face. Then, the 2D nucleation should be the effective mechanism of formation of (00.1) twinned crystals, at low supersaturation.

In order to obtain a correct estimate of Q_0, the γ_{TE} values at $T = 298$ K should be considered. Unfortunately, in our model the vibrational entropy due to the vibrational motion of atoms in the lattice was not taken into account; then we only estimated the twinning energy values at 0 K. However, such values should be slightly reduced by the vibrational contribution at 298 K and, as a consequence, even the Q_0 values above-reported should be slightly lowered.

4. Conclusions

In this paper, the "Four Twin Laws of Calcite", (10.4), (01.8), (01.2), and (00.1), were studied by performing geometry optimizations of 2D twinned slabs by means of the force field method (GULP). For the first time, to the authors' knowledge, the equilibrium geometry at 0 K of the twin boundary interfaces was calculated. It also resulted that the (10.4) and (01.8) interfaces relax more than the (01.2) and (00.1) ones. With the exception of the structure of the (00.1) twinned slab, tilting and rotation of the CO_3 groups were observed at the twin boundary interface, as well as variations of the Ca−O distances and $d_{hk.l}$ thickness.

Moreover, both twinning (γ_{TE}) and adhesion energies were determined. The values of γ_{TE} are 0.162, 0.183, 0.259, and 0.001 J/m^2 for the (10.4), (01.8), (01.2), and (00.1) twin laws, respectively. It is important to stress that these data were obtained at 0 K. In order to calculate the twinning energies a $T > 0$ K, it is necessary to take into account the vibrational motion of atoms (vibrational entropy). This is a thermodynamical quantity that may affect slightly the values of γ_{TE} reported above, as it depends on the difference of entropy between a twinned crystal and a perfect one, so we expect a slight difference in the vibration frequency spectra. Future calculations will be devoted to determine such vibrational contribution.

By using the estimated γ_{TE} values and the classical nucleation theory, we hypothesized that the 2D nucleation should be an effective mechanism of formation of (00.1) twinned crystals. Instead, the occurrence of the (10.4), (01.8), and (01.2) twins should be exclusively due to the 3D nucleation.

References

(1) Wenk, H. R.; Barber, D. J.; Reeder, R. J. Microstructures in Carbonates. In *Carbonates: Mineralogy and Chemistry*; Reeder, R. J., Ed.; Reviews in Mineralogy; Mineralogical Society of America: Blacksburg, VA, 1983; Vol. 11, pp 301−367.

(2) Weiss, L. E.; Turner, F. J. Some Observations on Translation Gliding and Kinking in Experimentally Deformed Calcite and Dolomite. In *Fracture and Flow of Rocks*; Heard, H. C., Borg, I. V., Carter, N. L., Raleigh, C. B., Eds.; American Geophysical Union Monograph; 1972; Vol. 16, pp 95−107.

(3) Barber, D. J.; Wenk, H. R. *Phys. Chem. Mineral.* **1979**, *5*, 141–165.

(4) Bueble, S.; Schmahl, W. W. *Phys. Chem. Mineral.* **1999**, *26*, 668–672.

(5) Paterson, M. S.; Turner, F. J. Experimental Deformation of Strained Calcite Crystals in Extension. In *Experimental and Natural Rock Deformation*; Paulitisch, P., Ed.; Springer: Berlin, 1970; pp 109−141.

(6) Pokroy, B.; Kapon, M.; Marin, F.; Adir, N.; Zolotoyabko, E. *Proc. Natl. Acad. Sci. U.S.A.* **2007**, *104*, 7337–7341.

(7) Tasker, P. W. *J. Phys. C: Solid State Phys.* **1979**, *12*, 4977–4984.

(8) Pojani, A.; Finocchi, F.; Noguera, C. *Appl. Surf. Sci.* **1999**, *142*, 177–181.
(9) Wander, A.; Schedin, F.; Steadman, P.; Norris, A.; McGrath, R.; Turner, T. S.; Thornton, G.; Harrison, N. M. *Phys. Rev. Lett.* **2001**, *86*, 3811–3814.
(10) Bruno, M.; Massaro, F. R.; Prencipe, M. *Surf. Sci.* **2008**, *602*, 2774–2782.
(11) Bruno, M.; Massaro, F. R.; Prencipe, M.; Aquilano, D. *Cryst.Eng. Comm.*, in press.
(12) Hartman, P. *Bull. Soc. Franç. Minér. Crist.* **1959**, *82*, 158–163. Lacmann, R. Adsorption et Croissance Cristalline. In *Colloques Internationaux du Centre National de la Recherche Scientifique*; CNRS: Paris, 1965; Vol. 152, pp 195−214.
(13) Rohl, A. L.; Wright, K.; Gale, J. D. *Am. Mineral.* **2003**, *88*, 921–925.
(14) Gale, J. D. *J. Chem. Soc., Faraday Trans.* **1997**, *93*, 629–637.
(15) Becke, A. D. *J. Chem. Phys.* **1993**, *98*, 5648–5652.
(16) Dovesi, R.; Civalleri, B.; Orlando, R.; Roetti, C.; Saunders, V. R. Ab Initio Quantum Simulation in Solid State Chemistry. In *Reviews in Computational Chemistry*; Lipkowitz, B. K., Larter, R., Cundari, T. R., Eds.; John Wiley and Sons Inc.: New York, 2005; Vol. 21, pp 1−125.
(17) Mutaftschiev, B. *The Atomistic Nature of Crystal Growth*; Springer: Berlin, Germany, 2001.
(18) Gay, D. H.; Rohl, A. L. *J. Chem. Soc., Faraday Trans.* **1995**, *91*, 925–936.
(19) Stranski, I. N.; Kaischew, R. *Z. Phys. Chem.* **1934**, *B26*, 100–113. Stranski, I. N.; Kaischew, R. *Z. Phys. Chem.* **1934**, *B26*, 114–116. Stranski, I. N.; Kaischew, R. *Z. Phys. Chem.* **1934**, *B26*, 312–316.
(20) Kern, R. *Bull. Soc. Franç. Minér. Crist.* **1953**, *76*, 336. Kern, R. *Bull. Soc. Franç. Minér. Crist.* **1961**, *84*, 292–311. Curien, H.; Kern, R. *Bull. Soc. Franç. Minér. Crist.* **1957**, *80*, 111–132.
(21) Simon, B. *Contribution à l'étude de la formation des macles de croissance*. Ph.D. Thesis, Université d'Aix-Marseille, France, **1968**.
(22) Friedel, G. *Leçons de Cristallographie*; Berger-Levrault: Paris, France, 1926.
(23) Goldschmidt, V. *Atlas der Kristallformen*; Universitätverlag: Heidelberg, Germany, 1923−1931; Vol. 1−9